Optics and Laser Technology 131 (2020) 106417

Contents lists available at ScienceDirect

Optics and Laser Technology

journal homepage: www.elsevier.com/locate/optlastec

Full length article

Spatial distribution of the fluorescence induced by femtosecond laser filamentation in ambient air

Jiabin Wu[a,c], Zhiyong Wu[c], Tao Chen[c], He Zhang[a,b], Yunfeng Zhang[a,b], Yun Zhang[a,b], Shuang Lin[a,b], Xiaoming Cai[a,b], Anmin Chen[a,b], Yuanfei Jiang[a,b], Suyu Li[a,b,*], Mingxing Jin[a,b,*]

[a] Institute of Atomic and Molecular Physics, Jilin University, Changchun 130012, China
[b] Jilin Provincial Key Laboratory of Applied Atomic and Molecular Spectroscopy, Jilin University, Changchun 130012, China
[c] Changchun Institute of Optics, Fine Mechanics and Physics, Chinese Academy of Sciences, Changchun 130033, China

HIGHLIGHTS

- N_2 and N_2^+ fluorescence shows different spatial distribution along the propagation direction.
- The intersystem crossing scheme dominates the formation of $N_2(C^3\Pi_u)$ in the low-intensity region.
- Excitation and ionization processes play different roles along the filament column.

ARTICLE INFO

Keywords:
Femtosecond filament
Fluorescence
Spatial distribution
Intersystem crossing

ABSTRACT

Laser intensity has a great influence on the excitation, ionization and other dynamical processes of atoms and molecules. During the femtosecond laser filamentation, the different values of intensity along the propagation direction will have a great influence on the spatial distribution of the products generated by these processes, and that of the fluorescence emitted by these products. In this paper, by measuring the spatial distribution of fluorescence induced by femtosecond laser filament in air, we find that along the propagation direction, the fluorescence signal from N_2 appears in front of that from N_2^+. Based on the experimental observations, we discuss the mechanism for the formation of N_2 ($C^3\Pi_u$), and arrive at the conclusion that in the case of shorter focal length, the intersystem crossing process plays a main part in the formation of the $C^3\Pi_u$ state of N_2.

1. Introduction

Femtosecond laser filamentation in air has been a research hotspot in the past few decades. As the femtosecond laser pulses propagates in air, they will interact with the N_2 and O_2 molecules in air, and generate a large number of excited molecules, molecular nitrogen ions, atoms and atomic ions. After the complicated interaction between femtosecond laser pulse and atom, molecules, and light like fluorescence [1–3] and lasing [4–12], supercontinuum [13–18], and terahertz [19–21] etc. will be emitted from the filament region. By measuring the fluorescence spectra during the femtosecond filamentation, we can have an insight into the excitation, ionization and other dynamical processes which the molecules experience [22–24], and on this basis, we can obtain the laser intensity, electron temperature, plasma density and other information inside the femtosecond filament [25–27]. Furthermore, the backward propagating fluorescence induced by femtosecond filamentation have the advantage of high sensitivity, non-intrusiveness, and real-time analysis, making it possess promising application prospects in the remote sensing of atmospheric trace species [1,2].

In our work, we mainly focus on the fluorescence emission coming from the nitrogen molecules and molecular nitrogen ions, which is closely related to the dynamical processes that nitrogen molecules experience in the stronger laser filed, such as excitation, ionization and collision. For example, nitrogen molecules are ionized by the intense laser pulses, generating N_2^+ in different electronic states. For N_2 molecule, its ground state electronic configuration is $KK(\sigma_g 2s)^2(\sigma_u 2s)^2(\pi_u 2p)^4(\sigma_g 2p)^2$. According to the molecular orbital theory, removal of one electron from the HOMO (highest occupied molecular orbital), HOMO-1 and HOMO-2 of N_2 generates N_2^+ in the $X^2\Sigma_g^+$, $A^2\Pi_g$ and $B^2\Sigma_u^+$ electronic states, respectively. The laser intensity influences the excitation, ionization and other dynamical processes occurring in filament: when it is relatively low, excitation process may dominate the dynamical processes, when it is higher, the photo-

* Corresponding authors at: Institute of Atomic and Molecular Physics, Jilin University, Changchun 130012, China.
E-mail addresses: suyu11@mails.jlu.edu.cn (S. Li), mxjin@jlu.edu.cn (M. Jin).

https://doi.org/10.1016/j.optlastec.2020.106417
Received 4 December 2019; Received in revised form 10 May 2020; Accepted 12 May 2020

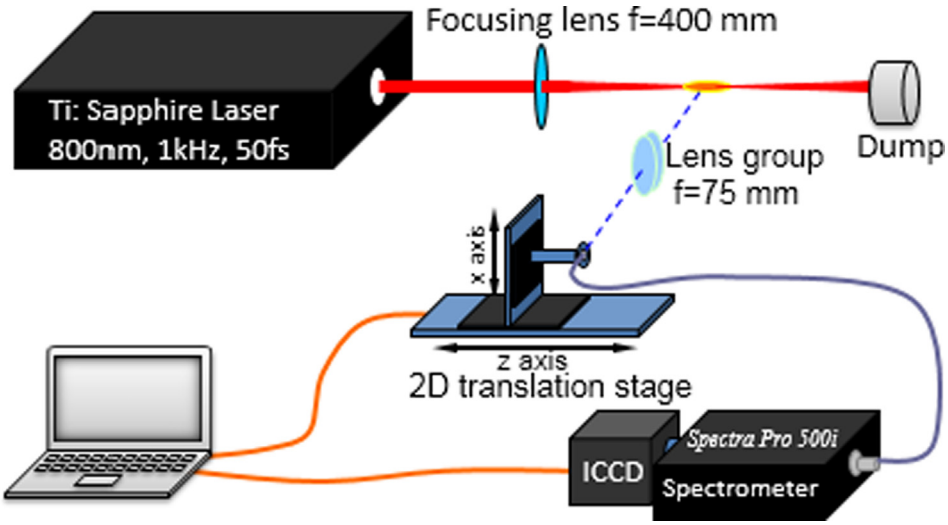

Fig. 1. Schematic diagram of the experimental setup for the measurement of side fluorescence induced by the femtosecond filament.

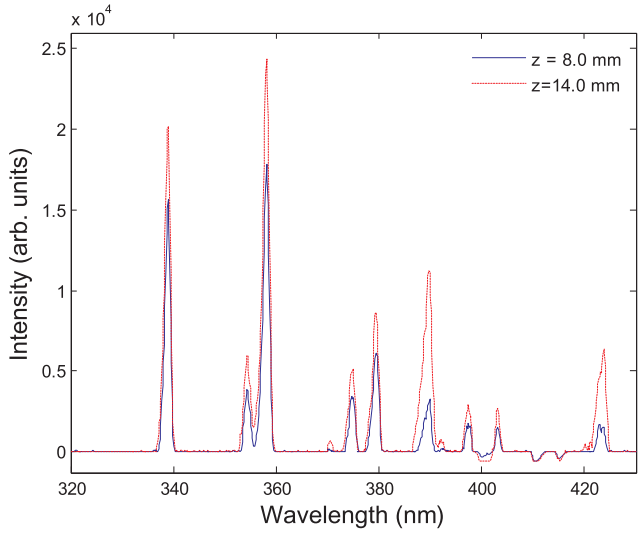

Fig. 2. Side fluorescence spectrum measured z = 8.0 mm and z = 14.0 mm. It should be noted that the position where the weakest fluorescence signal can be detected is set as z = 0 mm, and thus the propagation distance used is this paper is a relative value. The negative values at 400, 411 and 415 nm are caused by poor background.

ionization effect becomes obvious. Even for the photo-ionization, it can be classified as multiphoton ionization, above threshold ionization, and tunneling ionization *etc.* according to the parameters of laser pulse and those of the atoms and molecules [28]. During the femtosecond laser filamentation, along the propagation direction, the laser intensity firstly increases, then remain a relative high value for a certain distance and finally becomes weaker, which will inevitably affect the spatial distribution of the products formed by excitation and ionization processes and further that of the light emission from theses products.

In this paper, by measuring the spatial distribution of side emitted N_2 andN_2^+ fluorescence induced by femtosecond laser filamentation in air along the propagation direction, we analyze the excitation, ionization, collision and other process occurring in the femtosecond filament, and attempt to discuss the mechanism for the formation of N_2 ($C^3\Pi_u$).

2. Experimental setup

Fig. 1 shows the schematic diagram of experimental setup. We carry out the experiment by using a one-box ultrafast Ti: sapphire amplifier (Coherent Libra), and the central wavelength, duration and repetition rate of the laser pulses generated are 800 nm, 50 fs and 1 kHz, respectively. The laser beam passes through a lens with focal length of f = 400 mm, and generates filament in air. We measure the fluorescence spectra by the imaging approach: the produced fluorescence spectra are first collected by two lenses (fused silica f = 75 mm) placed on a two-dimension moving stage (x-z, where x denotes the vertical direction and z denotes the propagation direction), and then guided to a spectrometer (Spectra Pro 500i, PI Acton, and the grating is 150 grooves/mm) through an optical fiber. The fluorescence spectra are detected using an intensified charge coupled device (ICCD, PI-MAX, Princeton Instruments, 1024 × 1024 pixels). To obtain the spatial distribution of side fluorescence emission (x-z), the 2D moving stage is controlled by computer in the × and z directions, where the moving step in the × direction is 50 μm and that in the z direction is 100 μm.

3. Results and discussion

In this paper, we focus on the fluorescence emission from the second positive band system ($C^3\Pi_u \rightarrow B^3\Pi_g$ transition) of N_2 and the first negative band system ($B^2\Sigma_u^+ \rightarrow X^2\Sigma_g^+$ transition) of N_2^+. We select 337, 357, 380 nm spectral lines (corresponding to the $C^3\Pi_u(v = 0) \rightarrow B^3\Pi_g(v' = 0, 1, 2)$ transition) and 391, 428 nm spectral lines (corresponding to the $B^2\Sigma_u^+(v = 0) \rightarrow X^2\Sigma_g^+(v' = 0, 1)$ transition) to study the fluorescence from N_2 and N_2^+, as shown by the solid blue curve in Fig. 2. The femtosecond filament is generated by femtosecond laser pulse with energy of 3.2 mJ. It can be seen from Fig. 2(a) that at the propagation distance z = 8.0 mm, the 380 nm spectral line is stronger than the 391 nm one, while at z = 14.0 mm, it is just the reverse: the 391 nm spectral line is stronger than the 380 nm one (see dashed red curve in Fig. 2), indicating that along the propagation direction, the spatial distribution of fluorescence signal from N_2 and N_2^+ is different from each other.

Using a two-dimension moving stage shown schematically in Fig. 1, the side emitted light spectra in the x-z plane is obtained. We select 337, 380, 391 and 428 nm spectral lines from the spectra and present their integral intensity in the x-z plane, and thus obtain the spatial distribution of side fluorescence emission induced by the femtosecond filament, as shown in Fig. 3(a-d). It can be seen from the figure that along the propagation direction, N_2 fluorescence appears firstly, and after several millimeters of propagation, N_2^+ fluorescence appears. Furthermore, the peak value of N_2 fluorescence also appears before that of N_2^+ fluorescence. From Fig. 3(a-d), we can see that the area where the fluorescence signal can be measured in the × direction is about

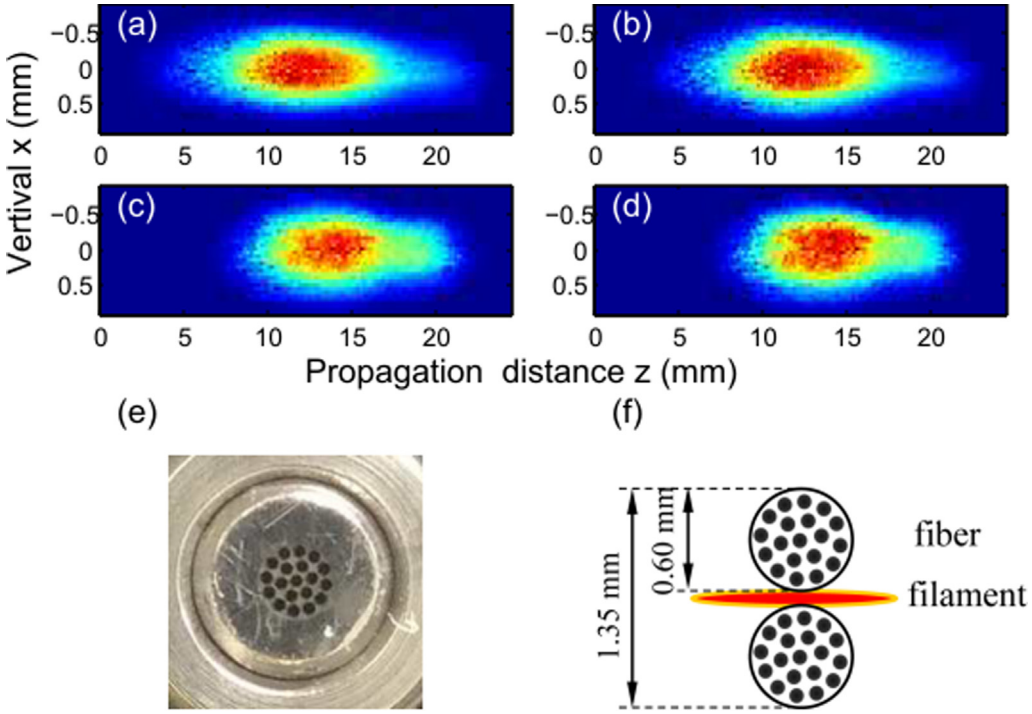

Fig. 3. Spatial distribution of (a) 337, (b) 380, (c) 391 and (d) 428 nm spectral lines, (c) photo of the head of optical fiber taken by a digital camera, (f) schematic diagram of optical fiber motion and filament.

1.35 mm, and this width is not the actual diameter of filament. The optical fiber that we use in the experiment consists of 19 cores (see Fig. 3(e)), and its diameter is 0.6 mm which is much larger than that of filament (around 100 μm). When it moves in the × direction, the coverage of the area when the fluorescence signal can be detected is about 1.35 mm, as shown in Fig. 3(f). The actual width of fluorescence emission is about 1.35 mm − 2*0.6 mm = 0.15 mm, which is consistent with the typical diameter of femtosecond filament (100 μm). In effect, to obtain the actual spatial distribution of fluorescence emission in filament, deconvolution of the data shown in Fig. 3(a–d) should be done, which is too complicated for our cases. What is more, we mainly focus on the spatial distribution of fluorescence signal along the propagation direction. For these reasons, we do not conduct the deconvolution in this paper. In the following part, we use the fluorescence signal measured when the centers of optical fiber and femtosecond filament are at the same height to study its spatial distribution along the propagation direction, which corresponds to the fluorescence spectrum measured at x = 0 mm shown in Fig. 3(a–d).

Fig. 4(a) presents the variation of the intensity of 337, 357, 380, 391 and 428 nm fluorescence signal with z. It can be clearly seen from the figure that the fluorescence signals from N_2 at 337, 357 and 380 nm appear at about z = 2.4 mm, then become stronger with increasing propagation distance and reach their maximal values at about z = 10 mm. In contrast, the fluorescence signals from N_2^+ at 391 and 428 nm appear at about z = 6.6 mm, and reach their maximal values at about z = 13.0 mm. After normalizing each spectral line in Fig. 4(a), we find that along the propagation direction, the variation of all the fluorescence from N_2 with z is identical to each other, and the variation tendency of all the fluorescence from N_2^+ is also identical to each other, as shown in Fig. 4(b). Due to distinct formation mechanisms of N_2^+ and N_2 fluorescence, their signals increase with the laser intensity at different orders of nonlinearity. We can estimate the axial laser intensity by the method proposed by Xu *et al.*, which is based on the signal ratio of two nitrogen fluorescence lines, i.e., 391 nm and 337 nm [25]:

$$I = 79 \times \left(\frac{2.6}{R} - 1\right)^{-0.34} \times 10^{12}\ \mathrm{W/cm^2} \quad (R = I_{391\mathrm{nm}}/I_{337}) \tag{1}$$

Since the 391 nm line appears at z = 6.6 mm and disappears at z = 23.1 mm, we can only calculate the axial intensity from z = 6.6 to z = 23.1 mm according to Eq. (1), as shown in Fig. 4(c). It can be seen from Fig. 4(c) that the laser intensity firstly increases and then decreases along the propagation direction, and the maximum value of intensity is about 1×10^{14} W/cm^2. It should be noted that this method can only roughly estimate the axial laser intensity.

Many previous papers have studied the axial filament fluorescence [23,26,29,30–32], and observed the difference between the spatial distribution of N_2 and N_2^+ fluorescence along the propagation axis. For example, Sun et al. measured the 391 nm and 337 nm fluorescence along the propagation axis, and found that the 391 nm lines increase greatly at the trail of femtosecond filament, and they attributed the phenomenon to the generation of a short pulse at trailing stage of the filamentation with reduced diameter [26]. However, in our experiment, the difference between N_2 and N_2^+ fluorescence mainly occurs at the beginning stage of femtosecond filamentation, while in the work of Sun et al., the 391 nm and 337 nm fluorescence shows identical change tendency.

Here, we attempt to analyze the discrepancy between the spatial distribution of N_2 and N_2^+ fluorescence according to the mechanism of the formation of N_2^+ ($B^2\Sigma_u^+$) and $N_2(C^3\Pi_u)$. As for N_2^+ ($B^2\Sigma_u^+$), it can be generated through two possible schemes: (1) photo-ionization (multi-photon or tunneling ionization) of the inner electron of N_2 in the strong laser field, and (2) ionization of N_2 via the collision with electron with high kinetic energy, i.e., $N_2(X^1\Sigma_g^+) + e \rightarrow N_2^+ (B^2\Sigma_u^+) + 2e$[29,33]. However, for $N_2(C^3\Pi_u)$, since the transition from the ground state $X^1\Sigma_g^+$ to the excited state $C^3\Pi_u$ is forbidden, $N_2(C^3\Pi_u)$ can not be generated directly. Three possible schemes have been proposed to explain its formation: (1) dissociative recombination through the processes: $N_2 + N_2^+ \rightarrow N_4^+$, $N_4^+ + e \rightarrow N_2(C^3\Pi_u) + N_2$ [34], (2) collision-assisted intersystem crossing, i.e., $N_2 + m\hbar\omega_0 \rightarrow N_2^*$, $N_2^* \xrightarrow{\mathrm{ISC}} N_2(C^3\Pi_u)$[35], and (3) impact excitation of N_2 by electron with high kinetic energy, i.e., $N_2(X^1\Sigma_g^+) + e \rightarrow N_2(C^3\Pi_u) + e$ [29,33]. The impact excitation scheme for the formation of $N_2(C^3\Pi_u)$ can be firstly excluded: The premise of generating $N_2(C^3\Pi_u)$ via impact excitation (i.e.,

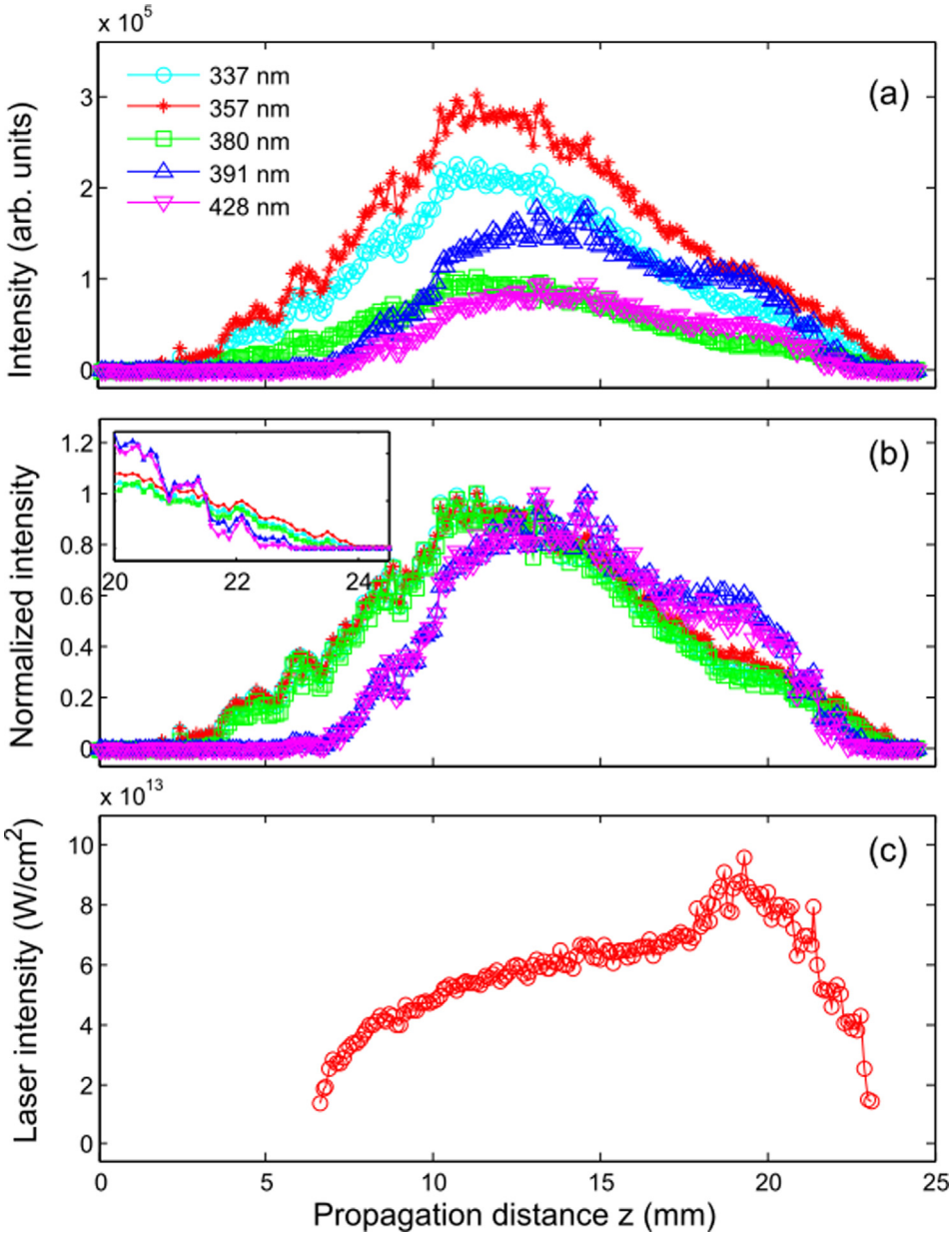

Fig. 4. (a) Variation of the intensity of 337, 357, 380, 391 and 428 nm fluorescence signal with z, (b) variation of the normalized intensity of 337, 357, 380, 391 and 428 nm fluorescence signal with z, (c) axial intensity distribution calculated through the signal ratio of 391 nm and 337 nm fluorescence lines [25]. Insert: amplified normalized intensity of 337, 357, 380, 391 and 428 nm fluorescence signal from 20 to 25 mm.

$N_2(X^1\Sigma_g^+) + e \rightarrow N_2(C^3\Pi_u) + e)$ is the existence of electrons with high kinetic energy which comes from the ionization of N_2. N_2^+ is generated during the ionization of N_2, which emits characteristic N_2^+ fluorescence. Therefore, if the impact excitation mechanism dominates the formation of $N_2(C^3\Pi_u)$, N_2 fluorescence can not appear in front of N_2^+ fluorescence along the laser propagation direction, which is obviously different from our experimental observation. Consequently, the impact ionization/excitation mechanism fails to explain the discrepancy between the spatial distribution of N_2 and N_2^+ fluorescence along the laser propagation direction.

As for the experiments in this paper, under the combined action of focusing lens and optical Kerr effect, the femtosecond filament is formed in front of the geometric focus of the focusing lens (F_g), as shown in Fig. 5(a). Here, we name the pulse collapse position as the realistic focus (F_r). For clarity, we divide the filamentation process along the propagation direction into five regions, as shown by I, II, III, IV and V in Fig. 5 (a). The solid black curve in Fig. 5(b) shows the evolution of laser intensity along propagation direction. After passing through the focusing lens, the intensity of laser beam becomes higher, and when it reaches a certain value, it is able to ionize the molecules in air, generating plenty of plasmas which defocus the laser beam. When the focusing and plasma defocusing effects reach a dynamical balance, filament is formed, and the intensity in filament is clamped to 10^{13}-10^{14} W/cm^2 (region III). Fig. 5(b) shows the evolution of laser intensity with the propagation distance. Since the laser intensity has a great influence on the dynamical processes like excitation and ionization, the spatial distribution of laser intensity along the propagation direction will result in different dynamical processes.

Ran et al. explained the different distributions of N_2 and N_2^+ fluorescence along the propagation direction through the dissociative recombination scheme [23]. The binding energies for the HOMO, HOMO-1, HOMO-2 are 15.58, 17.07 and 18.75 eV, respectively. Since the ionization rate decays exponentially with the electron binding energy, electron in the HOMO is firstly removed. When the laser pulse is a

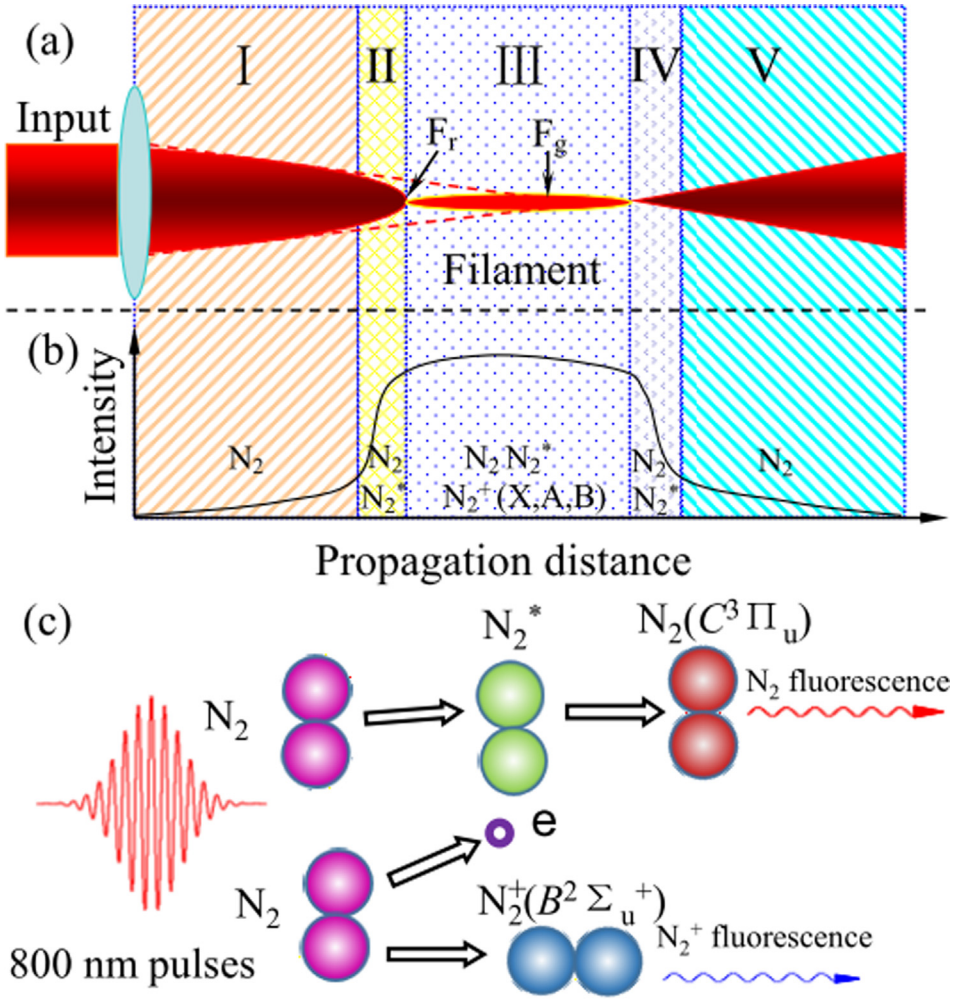

Fig. 5. Schematic diagram of (a) femtosecond filamentation with the aid of external focusing lens, (b) evolution of laser intensity with propagation distance and the main components existing in different regions, and (c) excitation and ionization of N_2 and accompanying fluorescence emission.

little far from F_r (i.e., in Region II), the laser intensity is not that high, most of the N_2^+ ions generated are in the $X^2\Sigma_g^+$ state, and then they experience the dissociative recombination process: $N_2^+(X^2\Sigma_g^+) + N_2 \rightarrow N_4^+$, $N_4^+ + e \rightarrow N_2(C^3\Pi_u)$ [24,34], generating numerous $N_2(C^3\Pi_u)$ molecules. As a result, in this region, only the N_2 fluorescence (337, 357 and 380 nm *etc.*) can be observed; in contrast, N_2^+ ($B^2\Sigma_u^+$) is only formed in the case of strong laser field, and therefore there is no N_2^+ fluorescence emission. Only when the laser pulse propagates to F_r (entering Region III), its intensity becomes high enough to generate N_2^+ ($B^2\Sigma_u^+$) directly, emitting the N_2^+ fluorescence at 391 and 428 nm *etc.*.

This explanation seems reasonable. However, the N_2^+ ($B^2\Sigma_g^+$) state can also be formed during the interaction of intense laser pulses with molecules, and the $X^2\Sigma_g^+$ state can not be formed alone. In our experiment, the focal length of lens used is $f = 400$ mm, which is in tightly focusing condition, the intensity inside filament is much higher than 5×10^{13} W/cm^2, the intensity of laser beam closer before the filament core (Region II, about 3 mm long) is still very high. Irradiated by such intense laser field, the ionized electron has large probability to re-collide with parent molecular ion, in this case, N_2^+ may be excited from the $X^2\Sigma_g^+$ state to the $B^2\Sigma_g^+$ state, resulting in the superradiance of nitrogen molecular ions [4]. In addition, spectrum broadening is obvious due to the high intensity of laser pulses, and thus multiphoton resonance effect is very easy to occur, which is also able to excite N_2^+ from the $X^2\Sigma_g^+$ state to the $B^2\Sigma_g^+$ state [5]. Through theoretical studies based on the Floquet theory, Zhang *et al.* reported that N_2^+ is preferentially generated at the peak of the laser electric filed and it will interact with the remaining part of the laser electric filed, which induces a nonresonant population transfer from the $X^2\Sigma_g^+$ state to the $B^2\Sigma_u^+$ state [6]. Furthermore, there exists a coupling among the $X^2\Sigma_g^+$, $A^2\Pi_g$ and $B^2\Sigma_u^+$ electronic states of N_2^+ [7–9]. Therefore, in the case of strong focusing condition, once the $X^2\Sigma_g^+$ state of N_2^+ is formed, the $B^2\Sigma_g^+$ state is formed almost at the same time. If the dissociative recombination scheme dominates the formation of $N_2(C^3\Pi_u)$, $N_2(C^3\Pi_u)$ and N_2^+ ($B^2\Sigma_u^+$) should be formed at the same position along the propagation direction, thus the fluorescence from N_2 andN_2^+ should appear together which is obviously contrary to our observations. Therefore, the dissociative recombination scheme can be excluded.

Here, we come to the intersystem crossing scheme. It requires the existence of intermediate singlet excited state, whose energy is close to that of the $C^3\Pi_u$ state. When N_2 undergoes the multiphoton absorption, it is possible to generate several kinds of singlet excited state whose energy is 12 eV above the $X^1\Sigma_g^+$ state [27]. Though it is difficult to make out which one is the needed singlet excited state, the pulse shaping study suggests that the intermediate (singlet excited) state is likely to take part in the formation of $N_2(C^3\Pi_u)$ [36]. Here, we exhibit the main components exist in the four regions shown in Fig. 5(a). In Region II, the laser intensity is relatively low which fails to ionize the N_2 molecules, but is able to excite N_2 molecules to the excited state, and thus generating a great many N_2^* in the excited singlet state. This is because the lowest energy needed to generate N_2^+ ($B^2\Sigma_u^+$) via the ionization of $N_2(X^1\Sigma_g^+)$ is 18.75 eV, which is higher than the energy needed in the formation of N_2^* (about 12 eV). Then the intersystem crossing process

occurs when N_2^* collides with N_2, generating a great many N_2 molecules in the $C^3\Pi_u$ state, and subsequently the transition from $C^3\Pi_u$ state to $B^3\Pi_g$ state occurs, emitting the characteristic N_2 fluorescence (337, 357 and 380 nm, *etc.*), as shown by the upper part in Fig. 5(c). As the laser pulse propagates to F_r (entering Region III), its intensity increases which is high enough to ionize N_2, generating N_2^+ ($B^2\Sigma_u^+$), and subsequently the $B^2\Sigma_g^+ \rightarrow X^2\Sigma_g^+$ transition occurs, emitting fluorescence from N_2^+ at 391 and 428 nm, as shown by the lower part in Fig. 5(c). In addition, with the increase of laser intensity, the ionization effect is enhanced while the excitation process is suppressed to some extent. As a result, when the N_2 fluorescence signals reach their maxima while the N_2^+ fluorescence signals keep on increasing, and consequently the maximal values of the N_2 fluorescence signals appear before those of the N_2^+ ones, as shown in Fig. 4. As the laser pulse propagates further, its intensity start to decrease (entering Region IV, i.e., the trail of the filament), it fails to ionize the N_2 molecules, but is able to excite N_2 molecules to the excited singlet state N_2^*. It can be seen from the insert in Fig. 4(b), the N_2^+ fluorescence disappears before N_2 fluorescence, which is similar to the case in the Region II. The above analyses suggest that the intersystem crossing scheme is not in contradiction with the experimental observations.

In our experiment, the discrepancy between the spatial distribution of N_2 and N_2^+ fluorescence can be attributed to the spatial distribution of laser intensity. Our analysis and discussion indicate that the intersystem crossing scheme plays a main role in the generation of N_2 fluorescence, at least in the case of shorter focal length, which is similar to the conclusion that we reported in the previous work [37–39]. It should be noted that we are not denying the dissociative recombination and the ionization/excitation mechanisms, for a great many molecular nitrogen ions and high energy electrons are generated in the filament core, and thus the dissociative recombination and ionization/excitation processes are also likely to occur.

4. Conclusion

In the process of femtosecond laser filamentation, the laser intensity firstly increases and then decreases along the propagation direction. Since laser intensity influence the excitation, ionization and other dynamical processes in the femtosecond filament, the spatial distribution of it makes that of the products formed by excitation and ionization processes different to each other. In this paper, it is found that spatial distribution of the N_2 fluorescence is different from that of theN_2^+ fluorescence. According to the experimental observations, we discuss the mechanism for the generation of $N_2(C^3\Pi_u)$. Our analysis shows that compared with the dissociative recombination scheme, the intersystem crossing scheme can better explain the experimental observations. The dissociative recombination and ionization/excitation processes may also occur in the femtosecond filament, however, at least in the shorter focal length cases, the intersystem crossing process plays a main role in the formation of $N_2(C^3\Pi_u)$. This study is helpful to the understanding for the mechanism of nitrogen fluorescence emission during the femtosecond laser filamentation in air.

CRediT authorship contribution statement

Jiabin Wu: Writing - original draft, Conceptualization. **Zhiyong Wu:** Formal analysis. **Tao Chen:** Visualization. **He Zhang:** Formal analysis. **Yunfeng Zhang:** Investigation. **Yun Zhang:** Methodology. **Shuang Lin:** Validation. **Xiaoming Cai:** Data curation. **Anmin Chen:** Methodology. **Yuanfei Jiang:** Software. **Suyu Li:** Supervision, Writing - review & editing, Methodology. **Mingxing Jin:** Supervision, Resources.

Declaration of Competing Interest

The authors declare that they have no known competing financial interests or personal relationships that could have appeared to influence the work reported in this paper.

Acknowledgements

This work was supported by the National Natural Science Foundation of China (Grant Nos. 11704145 and 11674124).

Appendix A. Supplementary material

Supplementary data to this article can be found online at https://doi.org/10.1016/j.optlastec.2020.106417.

References

[1] H. Xu, Y. Cheng, S.L. Chin, H.B. Sun, Femtosecond laser ionization and fragmentation of molecules for environmental sensing, Laser Photonics Rev. 9 (2015) 275.
[2] I. Dicaire, V. Jukna, C. Praz, C. Milián, L. Summerer, A. Couairon, Spaceborne laser filamentation for atmospheric remote sensing, Laser Photonics Rev. 10 (2016) 481.
[3] S. Mitryukovskiy, Y. Liu, P. Ding, A. Houard, A. Couairon, A. Mysyrowicz, Plasmaluminescence from femtosecond filaments in air: evidence for impact excitation with circularly polarized light pulses, Phys. Rev. Lett. 114 (2015) 063003.
[4] Y. Liu, P. Ding, G. Lambert, A. Houard, V. Tikhonchuk, A. Mysyrowicz, Recollision-induced superradiance of ionized nitrogen molecules, Phys. Rev. Lett. 115 (2015) 133203.
[5] S.L. Chin, H. Xu, Y. Cheng, Z. Xu, Natural population inversion in a gaseous molecular filament, Chin. Optic. Lett. 11 (2013) 013201.
[6] Y. Zhang, E. Lötstedt, K. Yamanouchi, Population inversion in a strong driven two-level system at far-off resonance, J. Phys. B 50 (2017) 185603.
[7] H. Xu, E. Lötstedt, A. Iwasaki, K. Yamanouchi, Sub-10-fs population inversion in N_2^+ in air lasing through multiple state coupling, Nat. Commun. 6 (2015) 8347.
[8] T. Ando, E. Lötstedt, A. Iwasaki, H. Li, Y. Fu, S. Wang, H. Xu, K. Yamanouchi, Rotational, Vibrational, and Electronic Modulations in N_2^+ Lasing at 391 nm: Evidence of Coherent $B^2\Sigma_u^+ - {}^X2_\Sigma{}^g + {}^-A_2\Pi u$ Coupling, Phys. Rev. Lett. 123 (2019) 203201.
[9] J. Yao, S. Jiang, W. Chu, B. Zeng, C. Wu, R. Lu, Z. Li, H. Xie, G. Li, C. Yu, Z. Wang, H. Jiang, Q. Gong, Y. Cheng, Population redistribution among multiple electronic states of molecular nitrogen ions in strong laser fields, Phys. Rev. Lett. 116 (2016) 143007.
[10] H. Zhang, C. Jing, J. Yao, G. Li, B. Zeng, W. Chu, J. Ni, H. Xie, H. Xu, S.L. Chin, K. Yamanouchi, Y. Cheng, Z. Xu, Rotational coherence encoded in an "air-laser" spectrum of nitrogen molecular ions in an intense laser field, Phys. Rev. X 3 (2013) 041009.
[11] H. Li, M. Hou, H. Zang, Y. Fu, E. Lötstedt, T. Ando, A. Iwasaki, K. Yamanouchi, H. Xu, Significant enhancement of N_2^+ lasing by polarization-modulated ultrashort laser pulses, Phys. Rev. Lett. 122 (2019) 013202.
[12] G. Point, A. Houard, A. Mysyrowicz, Y. Liu, Y. Brelet, Self-seeded lasing in ionized air pumped by 800 nm femtosecond laser pulses, Opt. Exp. 21 (2013) 22791.
[13] S.L. Chin, A. Brodeur, S. Petit, O.G. Kosareva, V.P. Kandidov, Filamentation and supercontinuum generation during the propagation of powerful ultrashort laser pulses in optical media (white light laser), J. Nonlinear Opt. Phys. Mater. 8 (1999) 121.
[14] V.P. Kandidov, O.G. Kosareva, I.S. Golubtsov, W. Liu, A. Becker, N. Akozbek, C.M. Bowden, S.L. Chin, Self-transformation of a powerful femtosecond laser pulse into a white-light laser pulse in bulk optical media (or supercontinuum generation), Appl. Phys. B 77 (2003) 149.
[15] J. Kasparian, M. Rodriguez, G. Méjean, J. Yu, E. Salmon, H. Wille, R. Bourayou, S. Frey, Y.B. André, A. Mysyrowicz, R. Sauerbrey, J.P. Wolf, L. Wöste, White light filaments for atmospheric analysis, Science 301 (2003) 61.
[16] X.L. Liu, X. Lu, X. Liu, L.B. Feng, J.L. Ma, Y.T. Li, L.M. Chen, Q.L. Dong, W.M. Wang, Z.H. Wang, Z.Y. Wei, Z.M. Sheng, J. Zhang, Broadband supercontinuum generation in air using tightly focused femtosecond laser pulses, Opt. Lett. 36 (2011) 3900.
[17] D.G. Jang, I.H. Nam, M.S. Kim, K. Kang, H. Suk, Generation of broadband supercontinuum light by double-focusing of a femtosecond laser pulse in air, Appl. Phys. Lett. 107 (2015) 131105.
[18] M. Vengris, N. Garejev, G. Tamosauskas, A. Cepenas, L. Rimkus, A. Varanavicius, V. Jukna, A. Dubietis, Supercontinuum generation by co-filamentation of two color femtosecond laser pulses, Sci. Rep. 9 (2019) 9011.
[19] Z.L. Zhang, Y.P. Chen, S. Cui, F. He, M. Chen, Z. Zhang, J. Yu, L.M. Chen, Z.M. Sheng, J. Zhang, Manipulation of polarizations for broadband terahertz waves emitted from laser plasma filaments, Nat. Photonics 12 (2018) 554.
[20] V.A. Andreeva, O.G. Kosareva, N.A. Panov, D.E. Shipilo, P.M. Solyankin, M.N. Esaulkov, P. González de Alaiza Martínez, A.P. Shkurinov, V.A. Makarov, L. Bergé, S.L. Chin, Ultrabroad terahertz spectrum generation from an air-based filament plasma, Phys. Rev. Lett. 116 (2016) 063902.
[21] P.A. Chizhov, A.A. Ushakov, V.V. Bukin, S.V. Garnov, Terahertz radiation from extended two-colour air filaments, Laser Phys. Lett. 16 (2019) 075301.
[22] M. Lei, C. Wu, Q. Liang, A. Zhang, Y. Li, Q. Cheng, S. Wang, H. Yang, Q. Gong, H. Jiang, The fast decay of ionized nitrogen molecules in laser filamentation investigated by a picosecond streak camera, J. Phys. B 50 (2017) 145101.
[23] P. Ran, G. Li, H. Tao Liu, S.N. Luo Hou, Collision-mediated ultrafast decay of N_2

fluorescence during fs-laser-induced filamentation, Opt. Exp. 27 (2019) 19177.
[24] P. Wang, S. Xu, D. Li, H. Yang, H. Jiang, Q. Gong, C. Wu, Spectroscopic study of laser-induced tunneling ionization of nitrogen molecules, Phys. Rev. A 90 (2014) 033407.
[25] S. Xu, X. Sun, B. Zeng, W. Chu, J. Zhao, W. Liu, Y. Cheng, Z. Xu, S.L. Chin, Simple method of measuring laser peak intensity inside femtosecond laser filament in air, Opt. Exp. 20 (2012) 299.
[26] X. Sun, S. Xu, J. Zhao, W. Liu, Y. Cheng, Z. Xu, S.L. Chin, G. Mu, Impressive laser intensity increase at the trailing stage of femtosecond laser filamentation in air, Opt. Express 20 (2012) 4790.
[27] J. Bernhardt, W. Liu, F. Théberge, H.L. Xu, J.F. Daigle, M. Chateauneuf, J. Dubois, S.L. Chin, Spectroscopic analysis of femtosecond laser plasma filament in air, Opt. Commun. 281 (2008) 1268.
[28] M. Protopapas, C.H. Keitel, P.L. Knight, Atomic physics with super-high intensity lasers, Rep. Prog. Phys. 60 (1997) 389.
[29] S. Mitryukovskiy, Y. Liu, P. Ding, A. Houard, A. Couairon, A. Mysyrowicz, Plasma luminescence from femtosecond filaments in air: Evidence for impact excitation with circularly polarized light pulses, Phys. Rev. Lett. 114 (2015) 063003.
[30] Q. Su, L. Sun, C. Chu, Z. Zhang, N. Zhang, L. Lin, Z. Zeng, O. Kosareva, W. Liu, S.L. Chin, Effect of molecular orbital angular momentum on the spatial distribution of fluorescence during femtosecond laser filamentation in air, J. Phys. Chem. Lett. 11 (2020) 730.
[31] Y. Liu, T. Wang, N. Chen, S. Du, J. Ju, H. Sun, C. Wang, J. Liu, H. Lu, S.L. Chin, R. Li, Z. Xu, Z. Wang, Probing the effective length of plasma inside a filament, Opt. Exp. 25 (2017) 11078.
[32] Y. Wei, Y. Liu, T.J. Wang, N. Chen, J. Ju, Y. Liu, H. Sun, C. Wang, J. Liu, H. Lu, S.L. Chin, R. Li, Spectroscopic analysis of high electric field enhanced ionization in laser filaments in air for corona guiding, High Power Laser Sci. Eng. 4 (2016) e8.
[33] Y. Itikawa, Cross sections for electron collisions with nitrogen molecules, J. Phys. Chem. Ref. Data 35 (2006) 31.
[34] H. Xu, A. Azarm, J. Bernhardt, Y. Kamali, S. Chin, The mechanism of nitrogen fluorescence inside a femtosecond laser filament in air, Chem. Phys. 360 (2009) 171.
[35] B.R. Arnold, S. Roberson, P.M. Pellegrino, Excited state dynamics of nitrogen reactive intermediates at the threshold of laser induced filamentation, Chem. Phys. 405 (2012) 9.
[36] J. Plenge, A. Wirsing, C. Raschpichler, M. Meyer, E. Rühl, Chirped pulse multiphoton ionization of nitrogen: Control of selective rotational excitation in N_2^+ ($B^2\Sigma_u^+$), J. Chem. Phys. 130 (2009) 244313.
[37] Y. Shi, A. Chen, Y. Jiang, S. Li, M. Jin, Influence of laser polarization on plasma fluorescence emission during the femtosecond filamentation in air, Opt. Commun. 367 (2016) 174.
[38] S. Li, Y. Jiang, A. Chen, L. He, D. Liu, M. Jin, Revisiting the mechanism of nitrogen fluorescence emission induced by femtosecond filament in air, Phys. Plasmas 24 (2017) 033111.
[39] S. Li, L. Sui, A. Chen, Y. Jiang, D. Liu, Z. Shi, M. Jin, Angular distribution of plasma luminescence emission during filamentation in air, Phys. Plasmas 23 (2016) 023102.